The influence of compositional change of $0.3Li_2MnO_3 \cdot 0.7LiMn_{1-x}Ni_yCo_{0.1}O_2$ $(0.2 \le x \le 0.5, y = x - 0.1)$ cathode materials prepared by co-precipitation

Ji-Hwa Jeong[a], Bong-Soo Jin[a], Woo-Seong Kim[b], Guoxiu Wang[c], Hyun-Soo Kim[a],*

[a] Battery Piezoelectric Research Center, Korea Electrotechnology Research Institute, 28-1, Seongju-dong, Changwon, Gyeongsangnam-do 641-120, Republic of Korea
[b] Daejung EM Co., Incheon 405-820, Republic of Korea
[c] School of Mechanical, Materials and Mechatronic Engineering, University of Wollongong, NSW 2522, Australia

ARTICLE INFO

ABSTRACT

Cathode materials prepared by a co-precipitation are $0.3Li_2MnO_3 \cdot 0.7LiMn_{1-x}Ni_yCo_{0.1}O_2$ $(0.2 \le x \le 0.4)$ cathode materials with a layered-spinel structure. In the voltage range of 2.0–4.6 V, the cathodes show more than one redox reaction peak during its cyclic voltammogram. The $Li/0.3Li_2MnO_3 \cdot 0.7LiMn_{1-x}Ni_yCo_{0.1}O_2$ $(x = 0.3, y = 0.2)$ cell shows the initial discharge capacity of about 200 mAh g^{-1}. However, when $x = 0.2$ and $y = 0.1$, the cell exhibits a rapid decrease in discharge capacity and poor cycle life.

© 2011 Elsevier B.V. All rights reserved.

1. Introduction

The rapid advancement of electronic devices and the widespread use of mobile devices have increased the demand for next generation battery technology. In particular, research on large-scale batteries for hybrid electric vehicles (HEVs) and electricity storage systems have focused on properties such as high energy density, high power density, high safety and low material costs. At present, $LiCoO_2$ has been widely using as an active material in lithium ion batteries. However it is an expensive and toxic material, thus limiting its potential. It also has a safety problem, in that oxidized Co^{4+} ions cause electrolytes to decompose at high potentials. Recently, some researchers have attempted to use transition metals as a substitute for $LiCoO_2$. These include olivine or spinel-typed $LiFePO_4$, $LiMn_2O_4$ [1–4], layered $LiMn_{1/3}Ni_{1/3}Co_{1/3}O_2$ [5–11], etc. Moreover, Yabuuchi and Ohzuku [12] reported that layered $LiMO_2$ (M = Mn, Ni, Co) delivers a discharge capacity of about 200 mAh g^{-1} over the 2.5–4.5 V range.

Thackeray et al. [13] synthesized $Li_2M'O_3 \cdot LiMO_2$ compounds, which contains a $Li_2M'O_3$ (M' = Mn, Ti, Zr) phase of known inactive material. Although the $Li_2M'O_3$ is inactive, it is changed to active material when Li_2O is removed above 4.5 V. When the lithium-ions are extracted from a $Li_2M'O_3$ phase, the lithium-ions can then move to the vacancies where they have been extracted from the $LiMO_2$ [14]. It was considered that the advantage would help cycling properties improve.

In this study, we reduced the quantity of cobalt in the cathode in order to lower the overall costs of the material by substituting of Mn and Ni in the precursor that was precipitated. The electrochemical performances were evaluated to understand the electrochemical properties and the synthesized Li_2MnO_3–$LiMO_2$ was then analyzed using a scanning electron microscope (SEM) and an X-ray diffraction (XRD) to understand its physical properties.

2. Experimental

The precursors of $0.3Li_2MnO_3 \cdot 0.7LiMn_{1-x}Ni_yCo_{0.1}O_2$ $(0.2 \le x \le 0.5, y = x - 0.1)$ materials were prepared by a co-precipitation. NaOH and NH_4OH solutions were added to a solution that contained stoichiometric amounts of manganese sulfate ($MnSO_4 \cdot H_2O$), nickel nitrate ($NiSO_4 \cdot 7H_2O$) and cobalt sulfate ($CoSO_4 \cdot 7H_2O$). The pH level was kept between 11 and 11.5 by controlling the amount of NaOH. The solution was strongly stirred in 500–1150 rpm. The particle size was controlled by the pH, reaction time and stirring speed. Spherical particles were uniformly produced for a pH level of 11, a reaction time of 24 h and a stirring speed of 1150 rpm. The precipitation filtrate was washed with distilled water to remove the residual impurity of OH$^-$, SO$_4{}^{2-}$, etc. Following this, the washed precursors were dried at 100 °C for 24 h in air. Ethanol was added into the mixture of
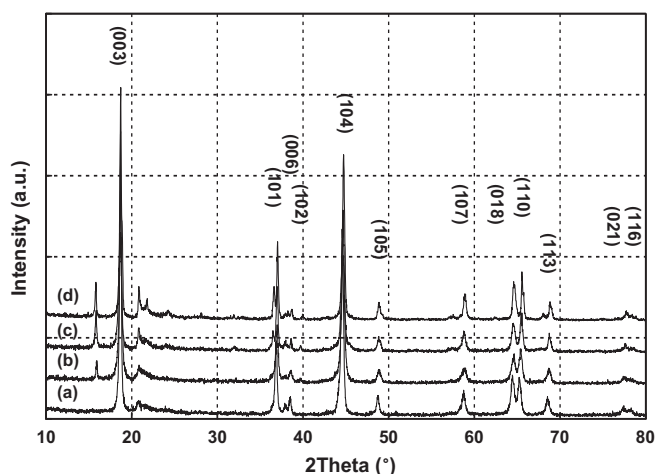
Fig. 1. XRD patterns of $0.3Li_2MnO_3 \cdot 0.7LiMn_{1-x}Ni_yCo_{0.1}O_2$ ($0.2 \le x \le 0.5$, $y = x - 0.1$) powders: (a) $x = 0.5$, (b) $x = 0.4$, (c) $x = 0.3$, and (d) $x = 0.2$.

Fig. 2. DSC profiles of $0.3Li_2MnO_3 \cdot 0.7LiMn_{1-x}Ni_yCo_{0.1}O_2$ ($0.2 \le x \le 0.5$, $y = x - 0.1$) cathode materials after charging to 4.6 V.

the precursor and then the lithium hydroxide was formed as a mud-like state. These mud-like mixtures were heat-treated at 500 °C for 5 h and then calcined at 800 °C for 3 h in air.

Powder XRD patterns of finely ground samples were collected at room temperature using a Philips PW1830 diffractometer with Cu Kα radiation ($\lambda = 1.5406$ Å). It was operated at a rate of 40 kV and 30 mA over a 2θ range of 10–80° in continuous scan mode at $0.04° s^{-1}$. Scanning electron microscope (SEM) images of $0.3Li_2MnO_3 \cdot 0.7LiMn_{1-x}Ni_yCo_{0.1}O_2$ ($0.2 \le x \le 0.5$, $y = x - 0.1$) were obtained by means of a Hitachi S-4800 machine. The thermal stability of samples was studied using differential scanning calorimetry (DSC). The cells were charged to 4.6 V and then they were opened in a dry room where the cathode electrodes were recovered from the aluminum foil. The DSC scan was carried out at a rate of $5 °C min^{-1}$ from 150 to 350 °C.

The electrodes were fabricated from 84:8:8 (mass %) mixture of active material:polyvinylidene difluoride (PVDF, Aldrich) as a binder:super-P carbon black (MMM Carbon) as a conducting agent. The PVDF was dissolved in N-methylpyrrolidinone (NMP, Kanto), and the active material including a conductor agent were added. After the homogenization process, the slurry was evacuated for 20 min to remove the retained air. The slurry was then coated on thin a aluminum foil (15 μm thick) and dried overnight at 100 °C. The electrodes was pressed (600–800 kg cm^{-2}) and punched into 15 mm diameter disks. The cells were assembled in 2032 coin type cells by stacking a lithium anode (−3.05 V vs. NHE), a polypropylene separator (Celgard®3501) containing a liquid electrolyte and a cathode in turn. The liquid electrolyte consisted of 1 M LiPF$_6$ in 1:1 ethylene carbonate (EC):dimethyl carbonate (DEC). The cells were charged and discharged by using a TOSCAT-3100 battery cycler at current rates of C/10, 1 C and 2 C, respectively, in the voltage range of 2.0–4.6 V. The cells were assembled in a dry room (dew point below −55 °C) and aged for 12 h before the first charge to ensure full absorption of the electrolytes into the electrodes.

3. Results and discussion

Fig. 1 shows the XRD patterns of the $0.3Li_2MnO_3 \cdot 0.7LiMn_{1-x}Ni_yCo_{0.1}O_2$ ($0.2 \le x \le 0.5$, $y = x - 0.1$) cathode materials prepared by co-precipitation. In this figure, all of samples are consistent with a typical layered-type structure with space group R-3m, the α-NaFeO$_2$ structure. This is considered to be the case due to the Miller indices (006,102) and (108,110) specific characteristics of the layered structure [15]. In addition, the appearance of weak reflection around $2\theta = 21°$ indicates

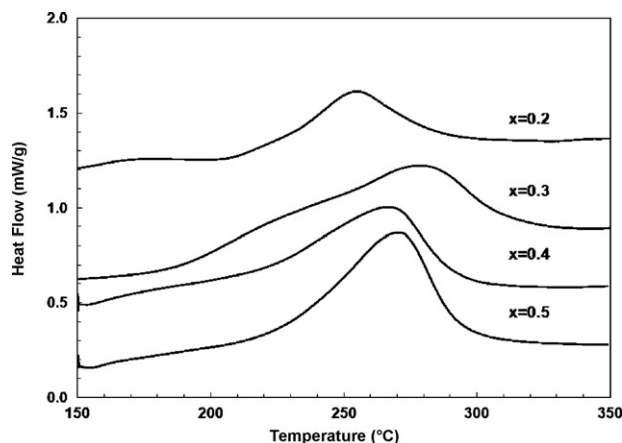Li$_2$MnO$_3$ phase having the monoclinic structure with space group C2/m. A comparison of Fig. 1(a) with (b)–(d) reveals that additional compounds in (b)–(d) are formed, which would be a LiMnO$_2$ of orthorhombic structure observed at $2\theta = 15°$ and 36°.

Fig. 2 shows the DSC curves of Li/$0.3Li_2MnO_3 \cdot 0.7LiMn_{1-x}Ni_yCo_{0.1}O_2$ ($0.2 \le x \le 0.5$, $y = x - 0.1$) prepared after charging to 4.6 V. For the range $x = 0.3$–0.5, exothermal heat appeared at around 270–280 °C. However, at $x = 0.2$, exothermal heat could be confirmed at a lower temperature of around 250 °C. This reaction can possibly be attributed to electrolyte oxidation caused by oxygen that is released from the cathode materials [16].

SEM images of the cathode materials prepared by co-precipitation and stirring for 24 h at room temperature are shown in Fig. 3. The $0.3Li_2MnO_3 \cdot 0.7LiMn_{1-x}Ni_yCo_{0.1}O_2$ ($0.2 \le x \le 0.5$, $y = x - 0.1$) powders revealed uniform particle distribution and similar particle size. All of the particles were well agglomerated and most were 5 μm in size with some small particles 1 μm size. However, it was difficult to see any measurable differences in surface morphologies due to compositional change.

Fig. 4 shows cyclic voltammogram (CV) curves of Li/$0.3Li_2MnO_3 \cdot 0.7LiMn_{1-x}Ni_yCo_{0.1}O_2$ ($0.2 \le x \le 0.5$, $y = x - 0.1$) cells. The CV testing was carried out with a potential sweep rate of $0.1 mV s^{-1}$ over the potential range from 2.0 to 4.6 V versus the Li electrode at room temperature. At the region near 4.1 V, the cathodes show identical oxidation peaks, which can be explained as being due to the extraction of lithium ions in the layered LiMO$_2$ (M = Mn, Ni, Co) structure. The reduction peaks corresponding with the above oxidation reaction that appeared in the 4 V range, were caused by an insertion of lithium ions into the MO$_2$ structure [17]. In addition, the oxidation peaks could be considered as due to the extraction reaction of lithium ions from the Li$_2$MnO$_3$ phase [18], which has been reported as an inactive material, but changes to an active state if it is operated above 4.5 V. Two side reactions at 2.7 V and 3 V are shown in Fig. 4(b)–(d). It is considered that the peaks are related to the orthorhombic structure of lithium manganese oxide, but the reactions below 3 V take place in. Guo et al. provided the spinel-type of LiMnO$_2$ phase take place in reactions below 3 V, as shown in the lower discharge plateaus [19]. The detailed mechanisms for oxidation and reduction of Li$_2$MnO$_3$–LiMO$_2$ during charge/discharge have already been reported.

Fig. 5 shows the voltage profiles of the Li/$0.3Li_2MnO_3 \cdot 0.7LiMn_{1-x}Ni_yCo_{0.1}O_2$ ($0.2 \le x \le 0.5$, $y = x - 0.1$) cells at room temperature. The Li/$0.3Li_2MnO_3 \cdot 0.7LiMn_{1-x}Ni_yCo_{0.1}O_2$ ($x = 0.3$) materials delivered the most discharge capacity, over 200 mAh g^{-1}. The first charge curve shows the two plateaus
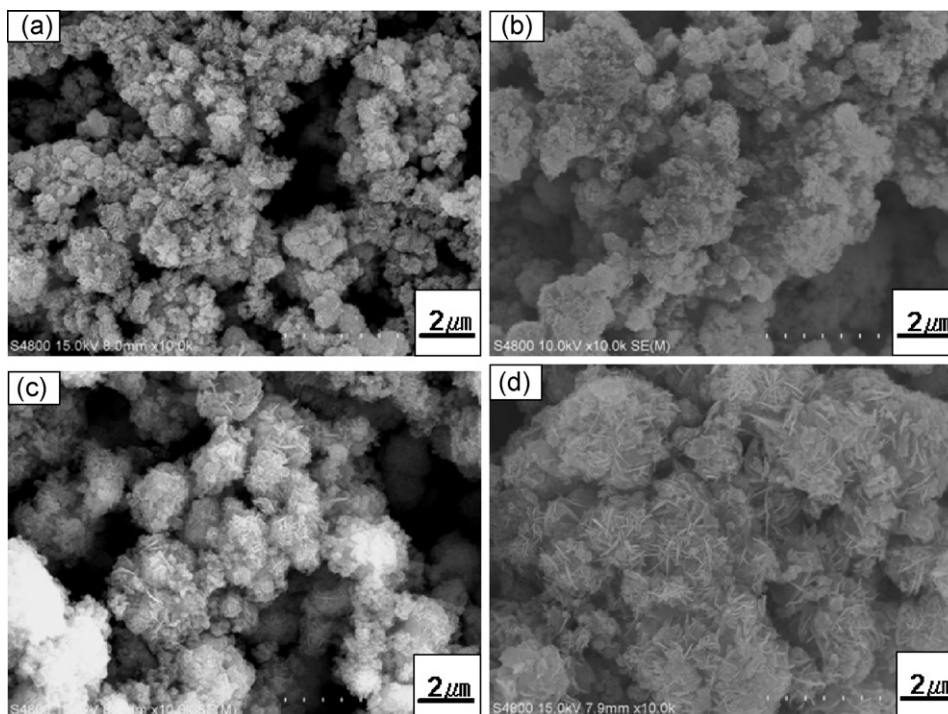
Fig. 3. Scanning electron micrographs of $0.3Li_2MnO_3 \cdot 0.7LiMn_{1-x}Ni_yCo_{0.1}O_2$ ($0.2 \leq x \leq 0.5$, $y = x - 0.1$) powders: (a) $x = 0.5$, (b) $x = 0.4$, (c) $x = 0.3$, and (d) $x = 0.2$.

at 4 and 4.5 V. The first charge capacity is $260 \, \text{mAh g}^{-1}$, implying a coulombic efficiency of 77%. On the other hand, $Li/0.3Li_2MnO_3 \cdot 0.7LiMn_{1-x}Ni_yCo_{0.1}O_2$ ($x = 0.2$) delivered a lower charge–discharge capacity due to the change of structure. The charge curves of all samples showed more than two reaction plateaus in the CV results, as shown in Fig. 4.

Fig. 6 shows the rate capability of $Li/0.3Li_2MnO_3 \cdot 0.7LiMn_{1-x}Ni_yCo_{0.1}O_2$ ($0.2 \leq x \leq 0.5$, $y = x - 0.1$) cells operated at the 0.1 C, 1 C and 2 C rates, respectively. All of the cells show poor rate capability at high current rate. Among them, the $Li/0.3Li_2MnO_3 \cdot 0.7LiMn_{1-x}Ni_yCo_{0.1}O_2$ ($x = 0.3$) cell had good discharge capacity at lower rates, but showed poor properties
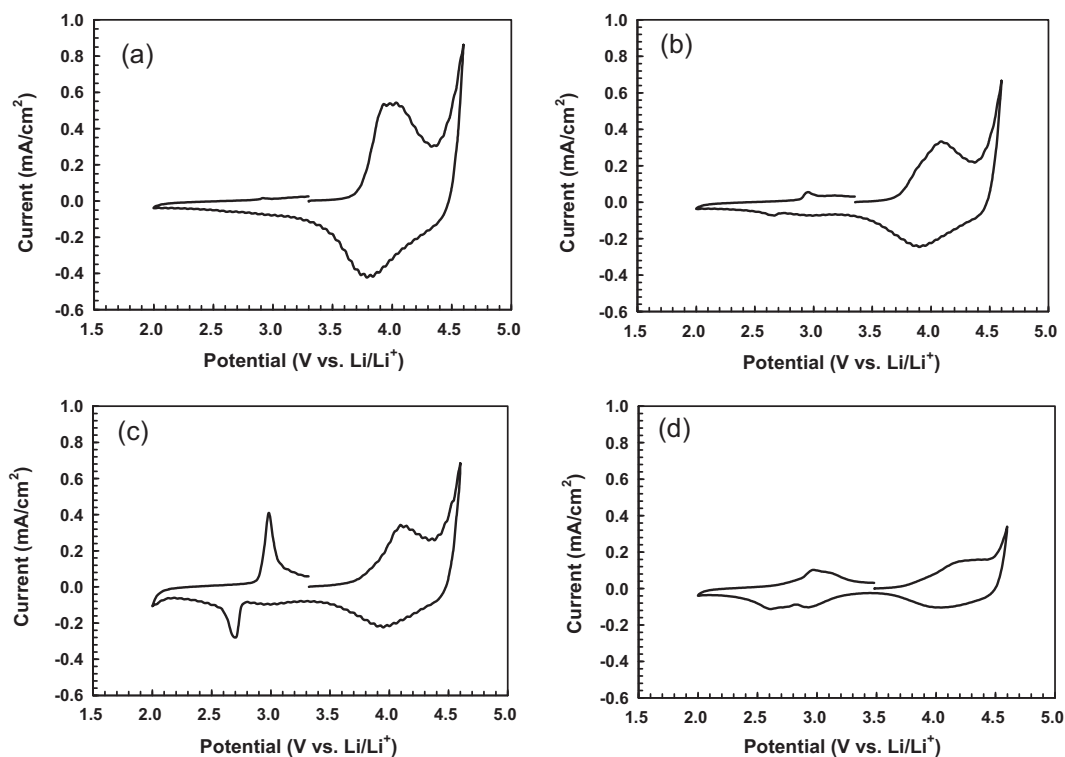

Fig. 4. Cyclic voltammograms of $Li/0.3Li_2MnO_3 \cdot 0.7LiMn_{1-x}Ni_yCo_{0.1}O_2$ ($0.2 \leq x \leq 0.5$, $y = x - 0.1$) cathode materials with $0.1 \, \text{mV s}^{-1}$ scan rate: (a) $x = 0.5$, (b) $x = 0.4$, (c) $x = 0.3$, and (d) $x = 0.2$.
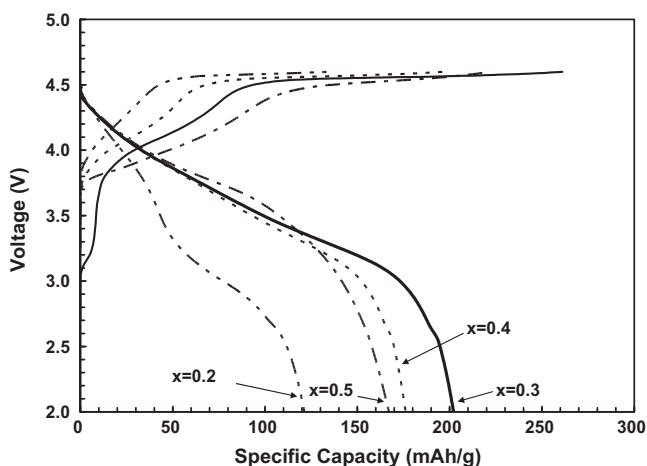
Fig. 5. Charge/discharge voltage profiles of $Li/0.3Li_2MnO_3 \cdot 0.7LiMn_{1-x}Ni_yCo_{0.1}O_2$ ($0.2 \leq x \leq 0.5$, $y = x - 0.1$) cells at the C/10 rate.

Fig. 7. Cycle-life performances of $Li/0.3Li_2MnO_3 \cdot 0.7LiMn_{1-x}Ni_yCo_{0.1}O_2$ ($0.2 \leq x \leq 0.5$, $y = x - 0.1$) cells operated between 2.0 and 4.6 V at the C/10 rate.

Fig. 6. Rate capability of $Li/0.3Li_2MnO_3 \cdot 0.7LiMn_{1-x}Ni_yCo_{0.1}O_2$ ($0.2 \leq x \leq 0.5$, $y = x - 0.1$) cells at the C/10, C/5, C/2, 1 C and 2 C rates.

below $50\,mAh\,g^{-1}$ discharge capacity. This might be due to the poor electronic conductivity, caused by higher Mn^{4+} content in the material.

Fig. 7 shows the cycle life properties of $Li/0.3Li_2MnO_3 \cdot 0.7LiMn_{1-x}Ni_yCo_{0.1}O_2$ ($0.2 \leq x \leq 0.5$, $y = x - 0.1$) when cycled between 2.0 and 4.6 V at 0.1 C. The $Li/0.3Li_2MnO_3 \cdot 0.7LiMn_{1-x}Ni_yCo_{0.1}O_2$ ($x = 0.3$) cell showed higher capacity retention of 95% from $188\,mAh\,g^{-1}$ discharge capacity after the 30th cycle. This composition had good cycle life properties, as well as the best first cycle discharge capacity. The $Li/0.3Li_2MnO_3 \cdot 0.7LiMn_{1-x}Ni_yCo_{0.1}O_2$ ($x = 0.4$) cell also showed discharge capacity retention of 84% as second best, but the $Li/0.3Li_2MnO_3 \cdot 0.7LiMn_{1-x}Ni_yCo_{0.1}O_2$ ($x = 0.2$) cell showed the worst cycling stability.

4. Conclusions

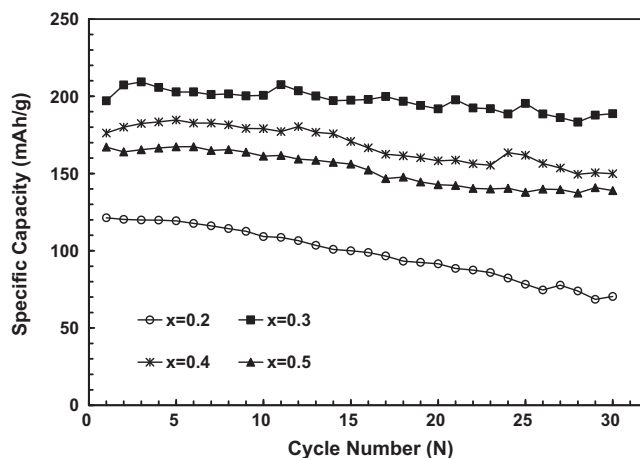Complex structure $0.3Li_2MnO_3 \cdot 0.7LiMn_{1-x}Ni_yCo_{0.1}O_2$ cathode materials were synthesized by a co-precipitation. The different compositions of cathode materials could be considered to compose a multi-structure, which is characterized by a layered and spinel structure. The cathode materials are agglomerated from small particles that are uniformly distributed. Various particle sizes of the powders are observed and most of them have 2–5 μm diameters. In the CV results, redox reaction peaks occur below 3 V, except when the composition is $x = 0.5$. This is due to the spinel structure. The first discharge capacity of the $Li/0.3Li_2MnO_3 \cdot 0.7LiMn_{1-x}Ni_yCo_{0.1}O_2$ cell ($x = 0.3$) was about $200\,mAh\,g^{-1}$ and showed good cycle life at room temperature. However, all of the samples showed poor rate performance at high current rate.

Acknowledgement

References

[1] A. Yamada, M. Tanaka, Mater. Res. Bull. 30 (1995) 715.
[2] M. Wakihara, L. Guohua, H. Ikuta, T. Uchida, Solid State Ionics 86 (1996) 907.
[3] T. Ohzuku, M. Kitagawa, T. Hirai, J. Electrochem. Soc. 137 (1990) 769.
[4] D. Song, H. Ikuta, T. Uchida, M. Wakihara, Solid State Ionics 117 (1999) 151.
[5] K. Shaju, B. Chowdari, Electrochim. Acta 48 (2002) 145.
[6] X. Liu, G. Zhu, K. Yang, J. Wang, J. Power Sources 174 (2007) 1126.
[7] D. Li, T. Muta, L. Zhang, M. Yoshio, H. Noguchi, J. Power Sources 132 (2004) 150.
[8] P. Hea, H. Wang, L. Qia, T. Osaka, J. Power Sources 160 (2006) 627.
[9] D. Li, Y. Sasaki, K. Kobayakawa, H. Noguchi, Y. Sato, Electrochim. Acta 52 (2006) 643.
[10] Y. Koyama, I. Tanaka, H. Adachi, Y. Makimura, T. Ohzuku, J. Power Sources 119 (2003) 644.
[11] Y. He, L. Pei, X. Liao, Z. Ma, J. Fluorine Chem. 128 (2007) 139.
[12] N. Yabuuchi, T. Ohzuku, J. Power Sources 119 (2003) 171.
[13] J.S. Kim, C.S. Johnson, M.M. Thackeray, Electrochem. Commun. 4 (2002) 205.
[14] S. Kang, M. Thackery, Electrochem. Commun. 11 (2009) 748.
[15] H. Liu, J. Li, Z. Zhang, Z. Gong, Y. Yang, Electrochim. Acta 49 (2004) 1151.
[16] Y. Baba, S. Okada, J.I. Yamaki, Solid State Ionics 148 (2002) 311.
[17] S. Park, Y. Sato, J. Kim, Y. Lee, Mater. Chem. Phys. 102 (2007) 225.
[18] C.S. Johnson, N.L. Christina Lefief, M.M. Thackeray, Electrochem. Commun. 9 (2007) 787.
[19] X. Guo, Y. Li, M. Zheng, J. Zheng, J. Li, Z. Gong, Y. Yang, J. Power Sources 184 (2008) 414.